Spatiotemporal visualization of wind turbulence from measurements by a Windcube 200s lidar in the atmospheric boundary layer

Anton Stephan, Norman Wildmann, Igor N. Smalikho

Anton Stephan, Norman Wildmann, Igor N. Smalikho, "Spatiotemporal visualization of wind turbulence from measurements by a Windcube 200s lidar in the atmospheric boundary layer," Proc. SPIE 10833, 24th International Symposium on Atmospheric and Ocean Optics: Atmospheric Physics, 1083357 (13 December 2018); doi: 10.1117/12.2504468

SPIE.

Event: XXIV International Symposium, Atmospheric and Ocean Optics, Atmospheric Physics, 2018, Tomsk, Russian Federation

Spatiotemporal visualization of wind turbulence from measurements by a Windcube 200s lidar in the atmospheric boundary layer

Anton Stephan[a], Norman Wildmann[a], Igor N. Smalikho*[b]

[a]Institute of Atmospheric Physics of the German Aerospace Center (DLR)
Münchener Straße 20, Oberpfaffenhofen, Wessling 82234 Germany
[b]V.E. Zuev Institute of Atmospheric Optics SB RAS
1, Akademik Zuev Square, Tomsk 634055, Russia

ABSTRACT

The results of spatiotemporal visualization of the kinetic energy of turbulence, its dissipation rate, and integral scale of turbulence from measurements by a Windcube 200s lidar with the use of the conical scanning by the probing beam in the atmospheric boundary layer are presented. When evaluating the parameters of wind turbulence, the lidar data filtering procedure was applied. This procedure allows obtaining acceptable results with a non-zero probability of bad estimate of the radial velocity.

Keywords: coherent Doppler lidar, wind turbulence

1. INTRODUCTION

A method for determination of wind turbulence parameters (kinetic energy of turbulence E, turbulence energy dissipation rate ε, and integral scale of turbulence L_V) from measurements by a micropulsed coherent Doppler lidar (MPCDL) with the use of the conical scanning by the probing beam and the elevation angle equal to φ = 35.3° was developed in [1]. This method was tested in a field experiment with the use of Stream Line MPCDL [2]. In that case, the wind turbulence parameters were determined from only those experimental data, for which the probability of bad (false) estimate of the radial velocity P_b was nearly zero. The probability P_b depends on the signal-to-noise ratio SNR, which is determined as the ratio of the average heterodyne signal power to the average detector noise power in a 50-MHz bandwidth. The lower SNR, the higher P_b [3-6]. To determine the wind speed and wind direction angle from the array of radial velocities measured at low SNR, when the probability P_b is significantly nonzero, the filtered sine-wave fitting (FSWF) procedure can be used [7]. However, the filtering of data measured by MPCDL has not been applied earlier for obtaining estimates of the turbulent parameters E, ε, and L_V.

In this paper, we propose a method for retrieval of wind turbulence parameters from lidar measurements with the procedure of filtering of good (representative) estimates of the radial velocity. The results of spatiotemporal visualization of turbulence in the atmospheric boundary layer, which were obtained by this method with the use of Windcube 200s MPCDL experimental data [8], are presented. The efficiency of the applied filtering is analyzed.

2. ESTIMATION OF WIND TURBULENCE PARAMETERS AT NONZERO PROBABILITY OF BAD ESTIMATE OF THE RADIAL VELOCITY

Let the conical scanning by the probing beam be used in the measurement by Windcube 200s MPCDL. The initial data of measurements by this lidar are represented by an array of signal power spectra $S(f; R_k, \theta_m, n)$, where f is frequency;

*smalikho@iao.ru; phone +7 3822 493595; fax +7 3822 492086

24th International Symposium on Atmospheric and Ocean Optics: Atmospheric Physics, edited by Gennadii G. Matvienko, Oleg A. Romanovskii, Proc. of SPIE Vol. 10833, 1083357

$R_k = R_0 + k\Delta R$ is the distance from the lidar to the center of the sensing volume; $k = 0,1,2,...,K-1$; ΔR is the range gate length; $\theta_m = m\Delta\theta$ is the azimuth angle; $m = 0,1,2,...,M-1$; M is the number of rays for one complete conical scan (θ_m varies from 0° to 360°); $\Delta\theta$ is the resolution in the azimuth angle, and $n = 1,2,3,...,N$ is the scan number [9]. Using the procedure described in [9], we obtained estimates of the radial velocity (projection of the wind velocity vector onto the axis of the probing beam) $\hat{V}_r(R_k,\theta_m;n)$ from the spectrum $S(f;R_k,\theta_m,n)$. The accuracy of these estimates depends on the signal-to-noise ratio SNR.

At arbitrary SNR, when the probability of bad estimate of the radial velocity P_b is nonzero, $\hat{V}_r(R_k,\theta_m;n)$ should be represented in the form [10-12]

$$\hat{V}_r(R_k,\theta_m;n) = \begin{cases} V_a(R_k,\theta_m;n) + V_g(R_k,\theta_m;n) & \text{in the case of good estimate,} \\ V_b(R_k,\theta_m;n) & \text{in the case of bad estimate,} \end{cases} \quad (1)$$

where $V_a(R_k,\theta_m;n)$ is the radial velocity averaged over the sensing volume centered at the distance R_k from the lidar; $V_g(R_k,\theta_m;n)$ is the random instrumental error of good estimate of the radial velocity with zero mean and properties of white noise [3]; $V_b(R_k,\theta_m;n)$ is the bad estimate of the radial velocity. The bad estimate contains no information about the wind and takes any values in the chosen passband in a random way [3]. If the noise component of the spectrum of lidar signal is white noise, then the probability density function of bad estimate of the radial velocity is distributed uniformly in the velocity range $[-B_V/2, +B_V/2]$ ($B_V = (\lambda/2)B$, where λ is the wavelength of the probing radiation, and B is the frequency passband) [12].

The information about wind turbulence is contained in fluctuations $V_a'(R_k,\theta_m;n) = V_a(R_k,\theta_m;n) - < V_a(R_k,\theta_m) >$, where the angular brackets denote the ensemble averaging . Therefore, from an array of lidar estimates of the radial velocity, we should first calculate their fluctuations [1]

$$\hat{V}_r'(R_k,\theta_m;n) = \hat{V}_r(R_k,\theta_m;n) - < \hat{V}_r(R_k,\theta_m) >, \quad (2)$$

from which we can find the increments (in azimuth) of fluctuations of estimates of the radial velocity

$$\Delta\hat{V}_r'(R_k,\theta_m + l\Delta\theta;n) = \hat{V}_r'(R_k,\theta_m + l\Delta\theta;n) - \hat{V}_r'(R_k,\theta_m;n). \quad (3)$$

In Eq. (3), $l = 1, L << M$ and $m = 0,1,2,...,M-1-l$. In the case of nonzero probability P_b, when determining the average radial velocity $< \hat{V}_r(R_k,\theta_m) >$ in Eq. (2), it is necessary to apply the filtering of good estimates of the radial velocity, for example, by the method of filtered sine-wave fitting [7].

When the probability is $P_b = 0$, the estimate of the radial velocity is described by the top line in the right-hand side of Eq. (1). In this case, the variance $\sigma_L^2 = < [\hat{V}_r'(R_k,\theta_m;n)]^2 >$ and the azimuth structure function $D_L(l\Delta\theta) = < [\Delta\hat{V}_r'(R_k,\theta_m + l\Delta\theta;n)]^2 >$ averaged over all azimuth angles θ_m can be represented in the form [1]

$$\sigma_L^2 = \sigma_a^2 + \sigma_g^2, \quad (4)$$

$$D_L(l\Delta\theta) = D_a(l\Delta\theta) + 2\sigma_g^2, \quad (5)$$

where $\sigma_a^2 = < [V_a'(R_k,\theta_m;n)]^2 >$ is variance and $D_a(l\Delta\theta) = < [V_a'(R_k,\theta_{m'} + l\Delta\theta;n) - V_a'(R_k,\theta_m;n)]^2 >$ is the azimuth structure function of the radial velocity averaged over the sensing volume with the longitudinal dimension Δz and the transverse dimension $\Delta y_k = R_k \cos\varphi\,\Delta\theta$ ($\Delta\theta$ in radians), and $\sigma_g^2 = < [V_g(R_k,\theta_m;n)]^2 >$ is the instrumental error of good estimate of the radial velocity.

According to the algorithm described in [1], σ_L^2 and $D_L(l\Delta\theta)$ can be used to obtain the estimates of the wind turbulence parameters: ε, E, and L_V through the calculations by the equations

$$\varepsilon = \left[\frac{D_L(L\Delta\theta) - D_L(\Delta\theta)}{A(L\Delta y_k) - A(\Delta y_k)} \right]^{3/2}, \quad (6)$$

$$E = (3/2)\{\sigma_{\mathrm{L}}^2 - D_{\mathrm{L}}(\Delta\theta)/2 + \varepsilon^{2/3}[F(\Delta y_k) + A(\Delta y_k)/2]\}, \quad (7)$$

$$L_V = 0.38E^{3/2}/\varepsilon, \quad (8)$$

where the following condition should be fulfilled: $\max\{\Delta z, L\Delta y_k\} < L_V$. The values of $A(\Delta y_k)$, $A(L\Delta y_k)$, and $F(\Delta y_k)$ are calculated by the equations given in [1]. In addition, the estimate of the instrumental error σ_g can be obtained as [1]

$$\sigma_g = \sqrt{[D_{\mathrm{L}}(\Delta\theta) - \varepsilon^{2/3} A(\Delta y_k)]/2}. \quad (9)$$

At the nonzero probability P_b, for determination of wind turbulence parameters by Eqs. (6) - (8), the filtering of good estimates of the radial velocity is required. Toward this end, first it is necessary to find three probability density functions (PDFs) $p(V^{(1)})$, $p(V^{(2)})$, and $p(V^{(3)})$, whose arguments are random values: $V^{(1)} = \hat{V}_r'(R_k, \theta_m; n)$, $V^{(2)} = \Delta\hat{V}_r'(R_k, \theta_m + \Delta\theta; n)$, and $V^{(3)} = \Delta\hat{V}_r'(R_k, \theta_m + L\Delta\theta; n)$. The analysis of the signal power spectrum measured by the Windcube 200s lidar has shown that the noise component of the spectrum is close to the white noise within the chosen frequency bandwidth $B = 50$ MHz [9]. Consequently, the probability density function of $V_b(R_k, \theta_m; n)$ is close to the uniform distribution in the velocity range $[-B_V/2, +B_V/2]$. It is obvious that at $P_b \neq 0$ the values of $V^{(q)}$ (superscript $q = 1, 2, 3$) go beyond this range. In addition, the probability density functions of $V^{(q)}$ obtained with the use of bad estimates of the radial velocity $V_b(R_k, \theta_m; n)$ already have no uniform distribution.

For determination of PDF $p(V^{(q)})$ within the range $[-B_V/2, +B_V/2]$ and with the uniform distribution of PDF of $V^{(q)}$ obtained with bad estimates of the radial velocities, we used the following algorithm. The interval $[-B_V/2, +B_V/2]$ is divided into I channels each $\delta V = B_V/I$ thick. The value of $V^{(p)}$ can fall within any of these channels. Consequently for every n-th scan, we obtain the histogram $N_q(V_i; n)$, where the subscript q correspond to estimation of $V^{(q)}$ (see above), $V_i = (i - I/2)\delta V$ and $i = 0, 1, 2, ..., I-1$, through addition of unit in $N_q(V_i; n)$ at the corresponding i-th channel. Previously, the number

$$\hat{i} = [V^{(q)}/\delta V + I/2] \quad (10)$$

is determined, where the square brackets denote rounding up or down to the nearest whole number. The number of this channel is determined as

$$i = \begin{cases} |\hat{i} + 1|, \text{ if } \hat{i} < 0 \\ \hat{i}, \text{ if } 0 \le \hat{i} \le I-1 \\ 2(I-1) - \hat{i}, \text{ if } \hat{i} > I-1 \end{cases}. \quad (11)$$

Once the histogram $N_q(V_i; N)$ is obtained, PDF is calculated as

$$p(V^{(q)}) = \frac{N_q(V_i; N)}{\delta V \sum_{i=0}^{I-1} N_q(V_i; N)}. \quad (12).$$

We have tested this method for determination of PDF $p(V^{(q)})$ in the numerical experiment without regard for turbulent fluctuations of the wind velocity ($E = 0$). The algorithm of numerical simulation of random realizations $\hat{V}_r(R_k, \theta_m; n)$ at the arbitrary wind velocity U, probability of bad estimate P_b, and variance of good estimate σ_g^2 of the radial velocity is described in [13]. The red curves in Fig. 1 show PDFs $p(V^{(1)})$ and $p(V^{(2)})$ (in the absence of turbulent fluctuations of wind velocity $p(V^{(3)}) = p(V^{(2)})$) obtained in the numerical experiment with the procedure described by Eqs. (10)–(12) at $B_V = 38.575$ m/s, $U\cos\varphi = 10.7125$ m/s, $P_b = 0.5$, and $\sigma_g = 1$ m/s. For comparison, blue curves in this figure show the corresponding PDFs calculated without application of this procedure.

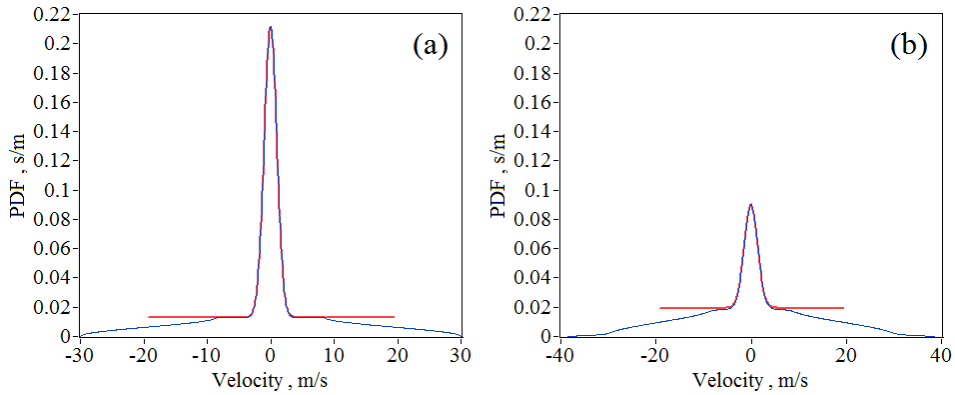

Figure 1. Probability density functions of fluctuations of estimates of the radial velocity $V^{(1)}$ (a) and differences in fluctuations of neighboring estimates of the radial velocity $V^{(2)}$ (b) obtained from the data of numerical simulation without (blue curves) and with (red curves) the procedure described by Eqs. (10) - (12).

It follows from the analysis of data shown by the red curves in Fig.1 that PDFs $p(V^{(q)})$ can be represented as a simple model $p_M(V^{(q)})$

$$p_M(V^{(q)}) = \frac{1-P_q}{\sqrt{2\pi}\sigma_q}\exp\left[-\frac{1}{2}\left(\frac{V^{(q)}}{\sigma_q}\right)^2\right] + \frac{P_q}{B_V}, \tag{13}$$

where the superscript q = 1, 2, and 3; σ_q^2 is the variance of good estimate, and P_q is the probability of bad estimate of $V^{(q)}$. Through the least-square fitting of the model PDF $p_M(V^{(q)})$ to PDF $p(V^{(q)})$ ($p_M(V^{(1)})$ and $p_M(V^{(2)})$ are shown by the red curves in Fig.1), we have obtained that $\sigma_1^2 = \sigma_g^2$ = 1 (m/s)^2, $\sigma_2^2 = \sigma_3^2 = 2\sigma_g^2$ = 2 (m/s)^2, $P_1 = P_b$ = 0.5, and $P_2 = P_3$ = 0.75.

We can generalize model PDF in the form (13) for the case of presence of turbulent fluctuations of the wind velocity in the atmosphere ($E \neq 0$) by taking $\sigma_1^2 = \sigma_a^2 + \sigma_g^2$, $\sigma_2^2 = D_a(\Delta\theta) + 2\sigma_g^2$, and $\sigma_3^2 = D_a(L\Delta\theta) + 2\sigma_g^2$. In addition, the least-square fitting of the model PDF $p_M(V^{(q)})$ to the measured PDF $p(V^{(q)})$ allows us to determine the variances σ_1^2, σ_2^2, and σ_3^2. Then, upon the replacement $D_{\mathrm{L}}(L\Delta\theta) - D_{\mathrm{L}}(\Delta\theta)$ with $\sigma_3^2 - \sigma_2^2$ in Eq. (6) and $\sigma_{\mathrm{L}}^2 - D_{\mathrm{L}}(\Delta\theta)/2$ with $\sigma_1^2 - \sigma_2^2/2$ in Eq. (7), Eqs. (6)–(8) are applied to calculate the wind turbulence parameters ε, E, and L_V. For determination of the instrumental error σ_g, $D_{\mathrm{L}}(\Delta\theta)$ should be replaced with σ_2^2 in Eq. (9).

A disadvantage of using model (13) in determination of turbulence parameters is that, actually, PDF of good estimate of $V^{(q)}$ (denote this PDF as $p_g(V^{(q)})$, and then $p(V^{(q)}) = (1-P_q)p_g(V^{(q)}) + P_q / B_V$) differs from the Gaussian distribution. Even if PDFs of the wind velocity components are distributed by the normal law, the distributions $p_g(V^{(2)})$ and $p_g(V^{(3)})$ are different from the Gaussian distribution. The numerical and field experiments have shown that this difference is relatively small, but it can lead to a regular error in estimation of the dissipation rate ε up to ~ 10–20%. Therefore, if the fitting of the model PDF $p_M(V^{(q)})$ to the measured PDF $p(V^{(q)})$ yielded the probability P_q = 0, then the parameters σ_{L}^2 and $D_{\mathrm{L}}(l\Delta\theta)$ entering into Eqs. (6) and (7) should be calculated directly, without the filtering procedure, since $\sigma_{\mathrm{L}}^2 = <[\hat{V}_r'(R_k, \theta_m; n)]^2>$ and $D_{\mathrm{L}}(l\Delta\theta) = <[\Delta\hat{V}_r'(R_k, \theta_m + l\Delta\theta; n)]^2>$. At $P_q \neq 0$, to find the variances σ_q^2 (subscript q = 1, 2, and 3), we can use the following algorithm, which does not require specification of model $p_g(V^{(q)})$:

$$\sigma_q^2 = \frac{1}{1-P_q} \int_{-\Delta V_q}^{\Delta V_q} dV^{(q)} [V^{(q)}]^2 [p(V^{(q)}) - P_q / B_V] . \quad (14)$$

Here, the integration limits $\pm\Delta V_q$ are taken equal to $\pm 3,5\tilde{\sigma}_q$, and the variance of good estimate $\tilde{\sigma}_q^2$ and the probability of bad estimate P_q are determined through the least-square fitting of the model PDF of $V^{(q)}$ to the measured one.

3. EXPERIMENT

The above method for determination of wind turbulence parameters from lidar measurements was tested in the field experiment conducted by us in October of 2017 in Oberpfaffenhofen. In this experiment, the Windcube 200s lidar was installed on the roof of the Institute of Atmospheric Physics of the German Aerospace Center (DLR). The measurements involved conical scanning by the probing beam at the elevation angle φ = 35.3°. The parameters of the lidar, measurement, and processing of data can be found in Table 1 of [9]. The method for obtaining estimates of the radial velocity, the signal-to-noise ratio, and the wind velocity vector from these measurements by the Windcube 200s lidar are also described in [9].

As a result of preprocessing of raw data measured by the lidar, we obtain three arrays of the values of $V^{(1)} = \hat{V}_r'(R_k, \theta_m; n)$, $V^{(2)} = \Delta\hat{V}_r'(R_k, \theta_m + \Delta\theta; n)$, and $V^{(3)} = \Delta\hat{V}_r'(R_k, \theta_m + L\Delta\theta; n)$ for every height $h_k = R_k \sin\varphi = h_0 + k\Delta h$, where the height step is Δh = 28.9 m. The duration of measurement at one azimuth angle was δt = 0.2 s. Since the number of rays M for one complete conical scan (when the azimuth angle θ_m varies from 0° to 360°) is 360, the duration of one scan $T_{\text{scan}} = M\delta t$ is 72 s (see Table 1 in [9]). To determine PDF $p(V^{(q)})$ (superscript q = 1, 2, and 3) and the wind turbulence parameters (ε, E, and L_V), we used the data measured for N = 25 conical scans, that is, for the time $T = NT_{\text{scan}}$ = 30 min. Thus, each of the probability density functions $p(V^{(q)})$ was calculated by the algorithm (10)–(12) from $N \times M$ = 9000 measured values of $V^{(q)}$.

We specified the number L based on the requirement $\max\{\Delta z, L\Delta y_k\} < L_V$. For the lidar used in this experiment, the longitudinal dimension of the sensing volume is Δz = 36 m, and the transverse dimension $\Delta y_k = R_k \cos\varphi \Delta\theta$ is a linear function of the distance from the lidar R_k (since φ = 25.3° and $\Delta\theta$ = 1°; at R_k, for example, equal to 100 m and 2 km, Δy_k is 2.8 m and 56.8 m, respectively). The known experimental data [1, 12, 14-16] can be used as *a priori* information about the integral scale L_V. In the atmospheric boundary layer (ABL) of intense turbulent mixing, L_V increases with height. As a rule, it does not exceed 500 m within ABL [14]. In our case, the number L should be no smaller than 2 and not exceeding 9 ($L\Delta\theta \le 9°$ [1]). For this condition to be true, L is a function of the distance R_k (or the height h_k).

Figure 2 shows examples of the probability density functions $p(V^{(q)})$ obtained from the experiment and the model PDFs $p_M(V^{(q)})$ described by Eq. (13) and fitted to the experimental ones. One can see that $p(V^{(q)})$ in these examples are rather close to $p_M(V^{(q)})$ both at the signal-to-noise ratios SNR providing zero probability of bad estimate of the radial velocity ((a – c) and (d – f)) and at low SNR, when $P_b \neq 0$ ((g – i) and (k – l)).

Figure 3 exemplifies PDFs $p(V^{(q)})$ and $p_M(V^{(q)})$ obtained from the lidar measurements at relatively high SNR and, correspondingly, at zero probability P_b. In contrast to the data shown in Figs. 2(a–c) and Figs. 2(d–f), here we can see significant deviations of $p_M(V^{(q)})$ from $p(V^{(q)})$. That is, the measured PDFs differ significantly from the Gaussian velocity distribution. Therefore, the variances σ_q^2 obtained through the least-square fitting of the model PDFs $p_M(V^{(q)})$ to the measured PDFs $p(V^{(q)})$ at P_b = 0 are inacceptable for estimation of the wind turbulence parameters, and we should determine σ_q^2 as $< [V^{(q)}]^2 >$ (that is, without application of the data filtering procedure).

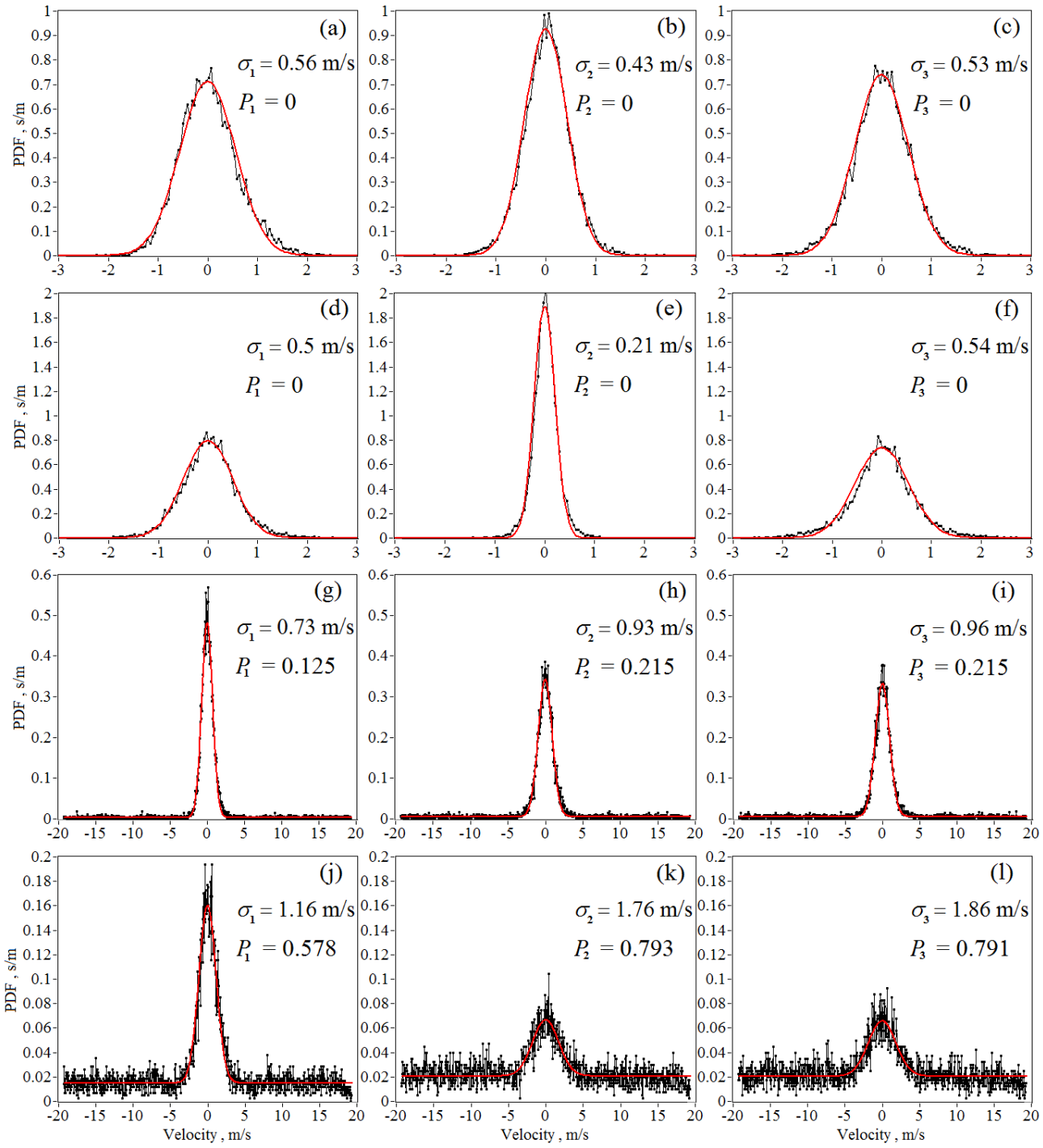

Figure 2. Probability density functions $p(V^{(1)})$ (a, d, g, j), $p(V^{(2)})$ (b, e, h, k), and $p(V^{(3)})$ (c, f, i, l) obtained from measurements by the Windcube 200s lidar in Oberpfaffenhofen from 13:20:53 to 13:50:53 Local Time on October 17 of 2017 at heights of 58 m at SNR = -16.5 dB (a - c), 404 m at SNR = -10.8 dB (d - f), 693 m at SNR = -19.8 dB (g - i), and 895 m at SNR = -24 dB (j - l) (dots connected by black curves). Red curves are for the corresponding model PDFs $p_M(V^{(q)})$ described by Eq. (13). The estimates of σ_q and P_q (q = 1, 2, and 3) are given near the plots.

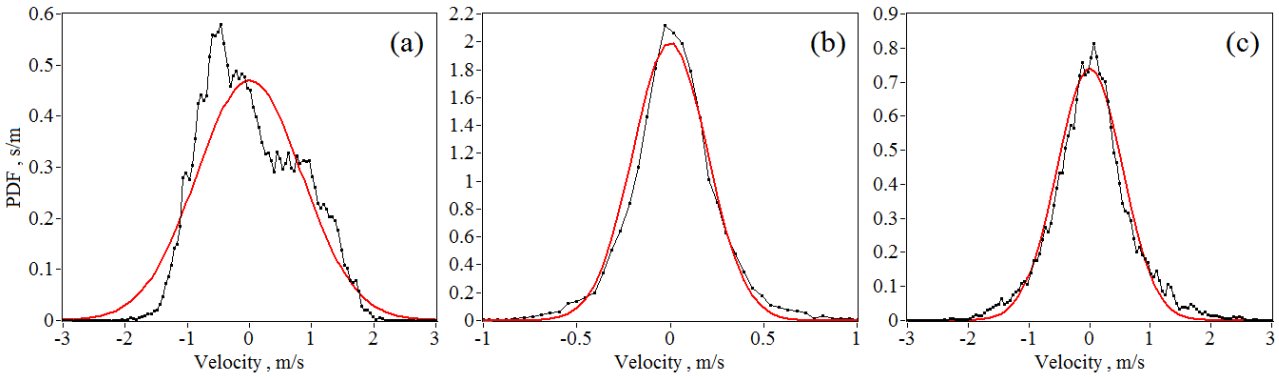

Figure 3. Probability density functions $p(V^{(1)})$ (a), $p(V^{(2)})$ (b), and $p(V^{(3)})$ (c) obtained from measurements by the Windcube 200s lidar in Oberpfaffenhofen from 12:08 to 12:28 Local Time on October 17 of 2017 at a height of 404 m at SNR = -8 dB (probability of bad estimate of the radial velocity $P_b = 0$) (dots connected by black curves). Red curves are for the corresponding model PDFs $p_M(V^{(q)})$ described by Eq. (13).

To obtain the distributions of the turbulent parameters $\varepsilon(h_k, t_n)$, $E(h_k, t_n)$, and $L_V(h_k, t_n)$ in height $h_k = h_0 + k\Delta h$ and in time $t_n = nT_{\text{scan}}$, where $h_0 = 57.8$ m, $k = 0, 1, 2, ..., 29$, and $n = 1, 2, 3, ...$, we used the raw data measured by the Windcube 200s lidar in Oberpfaffenhofen from 07:45 to 18:15 Local Time on October 17 of 2017. In addition to the mentioned wind turbulence parameters, the distributions of the signal-to-noise ratio $\text{SNR}(h_k, t_n)$, variances $\sigma_q^2(h_k, t_n)$, and probabilities $P_q(h_k, t_n)$ (subscript q = 1, 2, and 3) were obtained. Using Eq. (9), we have calculated the spatiotemporal distributions for the instrumental error of good estimate of the radial velocity $\sigma_g(h_k, t_n)$.

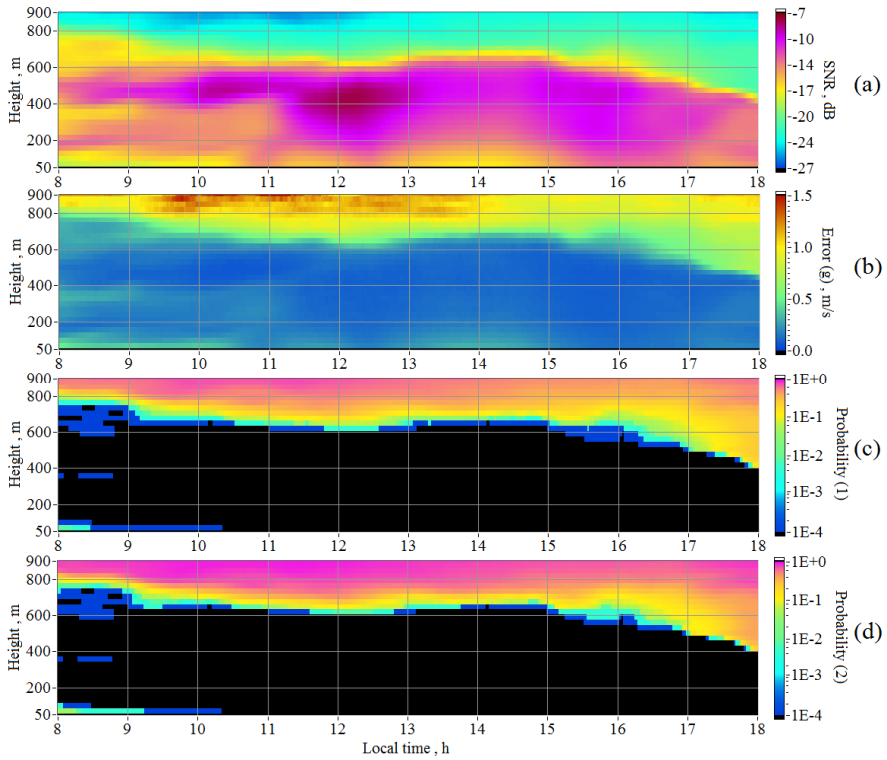

Figure 4. Height and time distributions of the signal-to-noise ratio SNR (a), error σ_g (b), and probabilities $P_1 \equiv P_b$ (c) and P_2 (d) obtained from measurements by the Windcube 200s lidar in Oberpfaffenhofen on October 17, 2017.

Figure 4 depicts the distributions of $\mathrm{SNR}(h_k,t_n)$, $\sigma_g(h_k,t_n)$, $P_1(h_k,t_n)$, and $P_2(h_k,t_n)$. Since $P_3 \approx P_2$, the results for $P_3(h_k,t_n)$ are omitted here. The black color in Figs. 4(c, d) means that the probability of bad estimate is $P_q = 0$ and the wind turbulence parameters can be determined without application of the procedure of filtering of the measured data. Within the area colored in black in Fig. 4(c), the signal-to-noise ratio SNR varies from -17 dB to -8 dB, while the instrumental error of good estimate of the radial velocity σ_g takes values from 0.06 m/s to 0.33 m/s (the smaller SNR, the larger σ_g). In the areas where $P_q \neq 0$, $P_b \equiv P_1$ varies from 10^{-4} to 0.75, SNR ranges from -15 dB to -26 dB, and σ_g takes values from 0.25 m/s to 1.5 m/s. The overlap of the variability ranges of SNR and σ_g at $P_q = 0$ and at $P_q \neq 0$ is explained by the random error of estimation of the considered parameters.

It should be noted that even if 9000 estimates of the radial velocity include only few bad estimates, without the filtering of measured data, they could cause a large error in determination of the dissipation rate ε, especially, in the case of weak turbulence. Our analysis has shown that the application of the filtering procedure does not allow the estimates of ε, E, and L_V to be obtained with an acceptable accuracy at SNR < -23 dB, $\sigma_g > 1$ m/s, and $P_b > 0.5$, even if turbulence is very strong. According to Fig.4, these conditions do not occur at $h_k \leq 800$ m. That is why we restricted our consideration to retrieval of vertical profiles of wind turbulence up to this height.

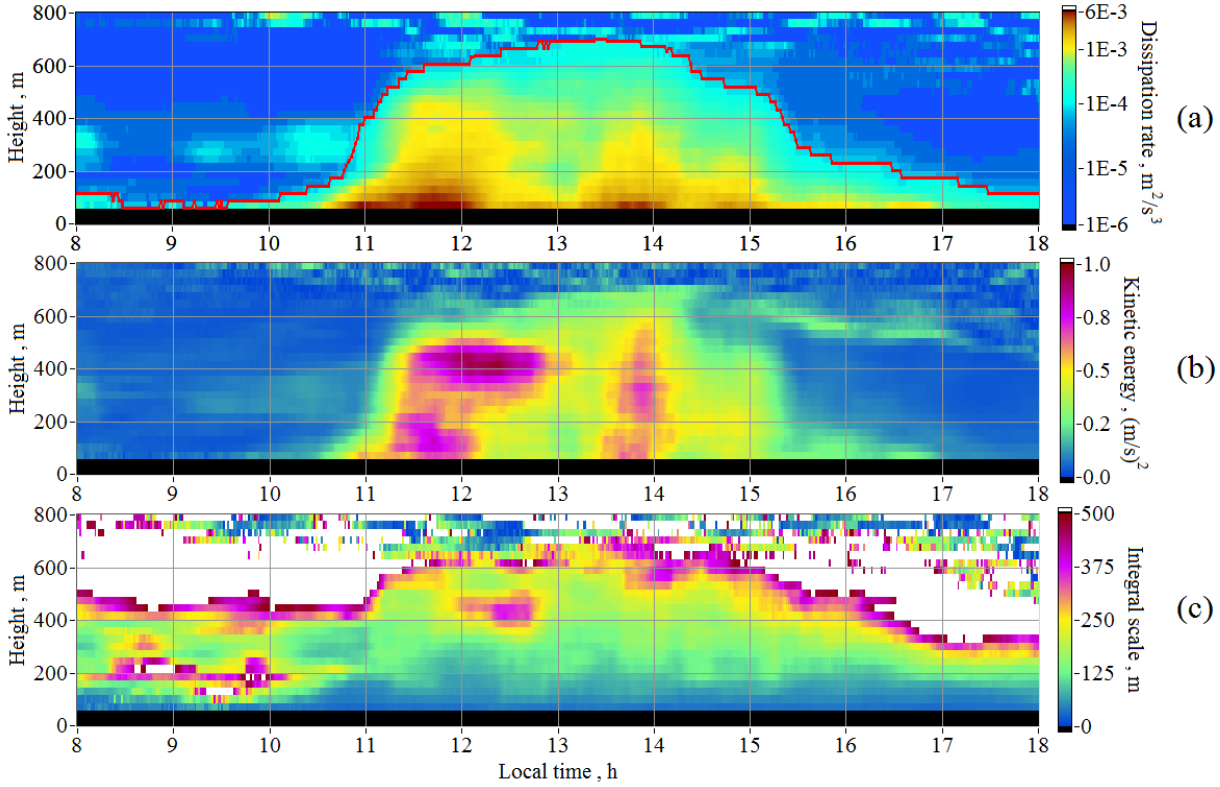

Figure 5. Height and time distribution of the turbulent energy dissipation rate (a), kinetic energy of turbulence (b), and integral scale of turbulence (c) obtained from measurements by the Windcube 200s lidar in Oberpfaffenhofen on October 17 of 2017.

Figure 5 shows the result of spatiotemporal visualization of wind turbulence in the form of two-dimensional distributions of $\varepsilon(h_k,t_n)$, $E(h_k,t_n)$, and $L_V(h_k,t_n)$. The white color in Fig.5(c) means that the estimate of the integral scale of turbulence exceeds 500 m. In the distributions for the dissipation rate and the kinetic energy, we can clearly see how the thickness of the layer of intense turbulent mixing of air masses changed in time, achieving approximately 700 m at the

maximum (at 13:30 Local Time). Some methods for determination of the thickness of the mixing layer h_{mix} have been developed earlier [17-21]. In contrast to these methods, we determined h_{mix} from the drop of the vertical profile $\varepsilon(h_k)$ down to the level of 10^{-4} m^2/s^3. The time dependence of the thickness of the mixing layer is shown by the red curve in Fig. 5(a). Despite the weak wind (1 - 2 m/s, see Fig.5 in [9]), the kinetic energy of turbulence at some instants increased up to 1 $(\text{m/s})^2$ at a height ~ 400 m, which is likely connected with strong convection. Inside the mixing layer, from 100 m to 500 m, the integral scale of turbulence L_V mostly increases monotonically in the range from 60 to 220 m with height. Outside the mixing layer, turbulence is weak (ε usually does not exceed 10^{-4} m^2/s^3).

In [1], the wind turbulence parameters were estimated from the data measured by the Stream Line lidar at zero probability P_b. As a result, we succeeded in retrieval of the vertical profiles of turbulence only up to 500 m, which is smaller than the maximum thickness of the mixing layer. The use of the filtering procedure in processing of the data measured by the Windcube 200s lidar has allowed us to obtain the results for the turbulence in the entire mixing layer and to determine its maximum thickness. According to the data shown in Fig.4 (b, c), without this procedure, we would succeed only in obtaining the results up to the maximal height of 600 m inside the mixing layer. According to our calculations with the use of numerical simulation, for the mixing layer the relative error of lidar estimates of ε, E, and L_V does not exceed, respectively, 7%, 10%, and 16%. The results obtained from measurements beyond this layer are less accurate. The weaker the wind turbulence, the higher the error of its lidar estimate. This is especially true for estimates of the integral scale of turbulence, which could be strongly overestimated (see the areas colored in white in Fig. 5(c)).

4. SUMMARY

Thus, in this paper we have proposed the method for determination of wind turbulence parameters from measurements by a pulsed coherent Doppler lidar with the use of the conical scanning by the probing beam under conditions of weak echo signal, when the probability of bad estimate of the radial velocity is nonzero. In the field experiment with the Wincube 200s lidar, this method was found to provide an acceptable result only when the probability of bad estimate of the radial velocity does not exceed 0.5. The procedure of filtering of good estimates of the radial velocity used in this method has allowed us to obtain the estimates of the turbulent energy dissipation rate, the kinetic energy of turbulence, and the integral scale of turbulence with relative errors not exceeding, respectively, 7%, 10%, and 16% within the entire layer of turbulent mixing of air masses, whose maximum height during the experiment achieved 700 m. Without application of this filtering procedure, the vertical profiles of the wind turbulence parameters can be retrieved to a maximum of 600 m.

Acknowledgments: The study was supported by the Ministry of Education and Science of the Russian Federation (Agreement No. 14.607.21.0151 - unique identifier RFMEFI60716X0151).

REFERENCES

[1] Smalikho, I. N. and Banakh, V. A., "Measurements of wind turbulence parameters by a conically scanning coherent Doppler lidar in the atmospheric boundary layer," Atmospheric Measurement Techniques 10(11), 4191–4208 (2017).
[2] Pierson, G., Davies, F., and Collier, C., "An analysis of performance of the UFAM Pulsed Doppler lidar for the observing the boundary layer," Journal of Atmospheric and Oceanic Technology 26(2), 240-250 (2009).
[3] Frehlich, R. G. and Yadlowsky, M. J., "Performance of mean-frequency estimators for Doppler radar and lidar," Journal of Atmospheric and Oceanic Technology 11(5), 1217-1230 (1994).
[4] Frehlich, R. G., "Simulation of coherent Doppler lidar performance in the weak-signal regime," Journal of Atmospheric and Oceanic Technology 13(6), 646-658 (1996).
[5] Frehlich, R. G., Hannon, S. M., and Henderson, S. W., "Coherent Doppler lidar measurements of winds in the weak signal regime," Applied Optics 36(15), 3491-3499 (1997).
[6] Frehlich, R. G., "Velocity error for coherent Doppler lidar with pulse accumulation," Journal of Atmospheric and Oceanic Technology 21(6), 905-920 (2004).

[7] Smalikho, I., "Techniques of wind vector estimation from data measured with a scanning coherent Doppler lidar," Journal of Atmospheric and Oceanic Technology 20(2), 276-291 (2003).
[8] Vasiljevic, N., Lea, G., Courtney, M., Cariou, J.-P., Mann, J., and Mikkelsen, T., "Long-Range WindScanner System," Remote Sensing 8(11), 896 (20016); doi:10.3390/rs8110896
[9] Stephan, A., Wildmann, N., and Smalikho, I. N. ,"Effectiveness of the MFAS method for determination of wind velocity vector from measurements by a Windcube 200s lidar," Atmospheric and Oceanic Optics, 2018 (accepted).
[10] Frehlich, R. G., "Effect of wind turbulence on coherent Doppler lidar performance," Journal of Atmospheric and Oceanic Technology 14(2), 54-75 (1997).
[11] Frehlich, R. G. and Cornman, L. B., "Estimating spatial velocity statistics with coherent Doppler lidar," Journal of Atmospheric and Oceanic Technology 19(3), 355-366 (2002).
[12] Banakh, V. A. and Smalikho, I. N., [Coherent Doppler wind lidars in a turbulent atmosphere], Artech House, Boston & London, 1-248 (2013).
[13] Banakh, V. A. and Smalikho, I. N., "Wind sensing in an atmospheric boundary layer by means of micropulse coherent Doppler lidars," Optics and Spectroscopy 121(1), 152-159 (2016).
[14] Byzova, N. L., Ivanov, V. N., and Garger, E. K., [Turbulence in Atmospheric Boundary Layer], Gidrometeoizdat, Leningrad, 263 p (1989).
[15] Monin, A. S., and Yaglom, A. M., [Statistical Fluid Mechanics, Volume II: Mechanics of Turbulence], M.I.T. Press, Cambridge, Mass., (1971).
[16] Lumley, J. L., and Panofsky, H. A., [The Structure of Atmospheric Turbulence], Interscience Publishers, New York, (1964).
[17] Hogan, R. J., Grant, A. L. M., Illingworth, A. J., Pearson, G. N., and O'Connor, E. J., "Vertical velocity variance and skewness in clear and cloud-topped boundary layers as revealed by Doppler lidar," Quarterly Journal of the Royal Meteorological Society 135(4), 635–643 (2009).
[18] Barlow, J. F., Dunbar, T. M., Nemitz, E. G., Wood, C. R., Gallagher, M. W., Davies, F., O'Connor, E. J., and Harrison, R. M., "Boundary layer dynamics over London, UK, as observed using Doppler lidar during REPARTEE-II," Atmospheric Chemistry and Physics 11(3), 2111–2125 (2011).
[19] Huang, M., Gao, Z., Miao, S., Chen, F., Lemone, M. A., Li, J., Hu, F., and Wang, L., "Estimate of boundary-layer depth over Beijing , China , using Doppler lidar data during SURF-2015," Boundary-Layer Meteorology 162(9), 503-522 (2017).
[20] Pichugina, Y. L. and Banta, R. M., "Stable boundary layer depth from high-resolution measurements of the mean wind profile," Journal of Applied Meteorology and Climatology 49(1), 20-35 (2010).
[21] Bonin, T. A., Carroll, B. J., Hardesty, R. M., Brewer, W. A., Hajny, K., Salmon, O. E., and Shepson, P. B., "Doppler lidar observation of the mixing height in Indianapolis using an automated composite fuzzy logic approach," Journal of Atmospheric and Oceanic Technology 35(3), 915-935 (2018).